

PARTITION GENERATIVE MODELING: MASKED MODELING WITHOUT MASKS

Justin Deschenaux^{1*}

Lan Tran¹

Caglar Gulcehre¹

¹EPFL, Lausanne, Switzerland

ABSTRACT

Masked generative models (MGMs) are widely used to capture complex data and enable faster generation than autoregressive models (AR) through parallel decoding. However, MGMs typically operate on fixed-length inputs, which can be inefficient: early in sampling, most tokens are masked and carry no information, leading to wasted computation. In contrast, AR models process only tokens generated previously, making early iterations faster. In this work, we introduce the Partition Generative Model (PGM), a novel approach that combines the strengths of AR and MGMs. Rather than masking, PGM partitions tokens into two groups and employs sparse attention to block information flow between them. Since there is no information flow between partitions, the model can process the previously-generated tokens only during sampling, while retaining the ability to generate tokens in parallel and in any order. On OpenWebText, PGMs offer at least 5 \times improvements in sampling latency and throughput, while producing samples with superior Generative Perplexity, compared to Masked Diffusion Language Models. On ImageNet, PGMs achieve a 7.5 \times higher throughput than MaskGIT, with only a slight increase in FID (5.54 vs. 5.35). With twice as many sampling steps, the FID reduces to 4.56 while being 3.9 \times faster than MaskGIT. Finally, PGMs integrate seamlessly with MGM distillation, providing further inference speedups.

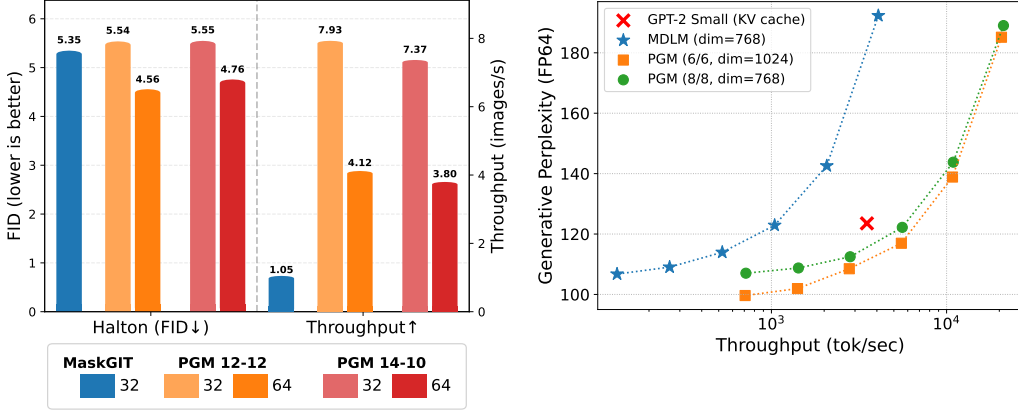


Figure 1: **(Left):** On ImageNet, using the Halton sampler, PGM (ours), reaches similar FID as MaskGIT with a 7.5 \times speedup. By sampling with twice as many steps, PGM reaches an FID of 4.56 while remaining 3.9 \times faster. **(Right):** On OpenWebText, PGM achieves a better Generative Perplexity with a 5.3 \times higher sampling throughput compared to MDLM, at a context length of 1024. The improvements come from our proposed novel neural network architecture.

1 INTRODUCTION

Masked generative models (MGM) excel at sampling from complex data distributions by iteratively denoising masked inputs. In fact, MGMs achieved remarkable success in various modalities, such

*Correspondence to justin.deschenaux@epfl.ch.

as images (Chang et al., 2022), video (Yu et al., 2023; Villegas et al., 2022), and audio (Comunità et al., 2024). Furthermore, recent advances in discrete diffusion (Austin et al., 2023; Campbell et al., 2022; Zhao et al., 2024; Lou et al., 2024; Sahoo et al., 2024; Shi et al., 2025; Ou et al., 2025) and discrete flow matching (Campbell et al., 2024; Gat et al., 2024) showed that MGMs can also be used in place of autoregressive models (ARM) for language modeling. The main advantage of MGMs over ARMs lies in their ability to (1) generate tokens in parallel, and (2) in any order, while ARMs are traditionally restricted to one-by-one, left-to-right decoding.

In practice, MGMs are implemented using Transformer variants with bidirectional attention (Vaswani et al., 2023; Peebles & Xie, 2023), which induces two important shortcomings compared to ARMs (Deschenaux & Gulcehre, 2024; Sahoo et al., 2024). First, during sampling, MGMs always process full-length sequences, even when most positions contain [MASK] tokens, to ensure consistency between training and sampling. In contrast, ARMs, thanks to their causal attention mechanism, process the previously generated tokens only. Secondly, during training, in a single forward pass, ARMs can learn from all but the first tokens. On the other hand, MGMs only learn to predict at masked positions. Hence, MGMs require more forward passes than ARMs to be exposed to as many tokens during training.

One way to increase the throughput of MGMs is to decode many tokens per step. However, this often leads to a substantial drop in sample quality. To reduce the number of sampling steps, often called *number of function evaluations* (NFE), while preserving quality, distillation (Deschenaux & Gulcehre, 2025; Zhu et al., 2025; Hayakawa et al., 2025; Sahoo et al., 2025a) can be employed. Distillation methods train a student model to match, in few steps, the behavior of a teacher with high NFE. However, distillation can reduce the diversity of samples (Gandikota & Bau, 2025). Instead of reducing the NFE, we improve the sampling speed by introducing *Partition Generative Models* (PGM), an alternative to MGMs, whose sampling steps are cheaper than MGM’s.

Instead of masking, PGMs partition tokens into two disjoint groups. Given the two groups, the denoiser learns to predict tokens in one group, based on the other, and vice-versa. This eliminates the need for [MASK] tokens. Importantly, the denoiser uses a constrained attention mechanism so that the two partitions do not interact during training. Therefore, a single partition (the clean tokens) are processed during sampling, just like for ARMs. Additionally, PGMs can learn from all input tokens, while retaining the parallel generation capabilities of MGMs.

On LM1B (Chelba et al., 2014), we show that PGMs achieve **a reduction of 1.95 in validation perplexity** compared to MGMs with the same number of layers. On OpenWebText (Gokaslan & Cohen, 2019), larger PGMs generate samples with lower Generative Perplexity than MDLM (Sahoo et al., 2024) while **achieving a 5 – 5.5 \times higher throughput** for a matching number of sampling steps. Importantly, we show that PGMs remain compatible with distillation methods designed for MGMs. On ImageNet, PGMs achieve slightly better FID than MaskGIT (Chang et al., 2022) with the original confidence-based sampler, and slightly worse with the Halton sampler (Besnier et al., 2025), suggesting broadly comparable quality. Importantly, **the sampling throughput of PGMs trained on ImageNet is about 7.5 \times higher than that of MaskGIT**, when using the same number of step.

2 BACKGROUND

2.1 GENERATIVE LANGUAGE MODELING

Language modeling addresses the task of generating sequences of discrete tokens (x_i) from a vocabulary $\mathcal{X} = \{0, \dots, N-1\}$. A language model generates sequences of length L , i.e. elements of $\mathcal{X}^L = \left\{ \mathbf{x}^{(i)} = (x_0^{(i)}, \dots, x_{L-1}^{(i)}) : x_j^{(i)} \in \mathcal{X} \right\}_{i=0}^{N^L}$. The training dataset $\mathcal{D} := \left\{ \mathbf{x}^{(0)}, \dots, \mathbf{x}^{(K-1)} : \mathbf{x}^{(i)} \in \mathcal{X}^L \right\}$ contains K such sequences. One fundamental objective of language modeling is to generate samples similar to those of the unknown distribution $p_{\text{data}} : \mathcal{X}^L \rightarrow [0, 1]$ that induced the training data set \mathcal{D} .

2.2 MASKED GENERATIVE MODELING

With MGMs, one of the integer in the vocabulary \mathcal{X} represent a special [MASK] token, absent from the samples in \mathcal{D} . The [MASK] represents a hidden value. During training, a subset of the tokens in

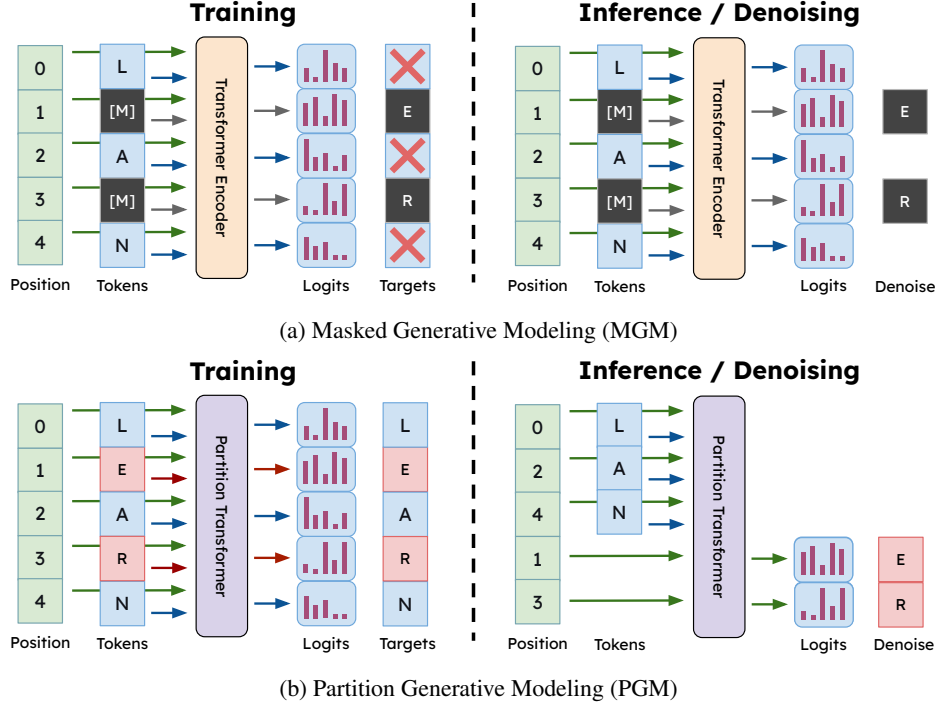


Figure 2: **Masked Generative Modeling (MGM) vs. Partition Generative Modeling (PGM).** **Training:** PGMs receive feedback at every position, while MGMs usually only apply loss to masked tokens. **Inference:** PGMs process only unmasked tokens, working with shorter sequences and predicting logits only for tokens to denoise. MGMs must process full-length sequences and compute logits at all positions. **Important note:** PGMs use a specialized architecture that ensures predictions for position i never depend on the token at position i .

$\mathbf{x} \in \mathcal{D}$ are replaced with **[MASK]**, and the model learns to reconstruct the masked positions. Formally, we train a denoiser $\mathbf{x}_\theta : \mathcal{X}^L \rightarrow \mathbb{R}^{L \times N}$, parameterized by θ , whose training objective is of the form:

$$\mathcal{L}_{\text{MGM}} := \mathbb{E}_{\mathbf{x} \sim \mathcal{D}, t \sim \mathcal{U}[0,1]} [w(t) \text{CE}(\mathbf{x}_\theta(\mathbf{z}_t; t), \mathbf{x})], \quad (1)$$

where t controls the fraction of tokens to mask. The corrupted sequence \mathbf{z}_t is obtained by independently masking each token with probability p_t (e.g., $p_t = t$ for simplicity). The weighting function $w : [0, 1] \rightarrow \mathbb{R}_{\geq 0}$ can emphasize certain noise levels over others. Finally, $\text{CE}(\hat{\mathbf{x}}, \mathbf{y})$ denotes the cross-entropy loss between predictions $\hat{\mathbf{x}}$ and target \mathbf{y} .

To generate samples, we begin with a sequence of **[MASK]** tokens. The model then iteratively refines the sequence, denoising a subset of masked positions at each step over multiple evaluations of \mathbf{x}_θ , following a fixed policy for selecting positions, e.g., at random or based on a confidence score.

2.3 MASKED DIFFUSION LANGUAGE MODELING

Masked Diffusion Language Models (MDLM; [Sahoo et al. \(2024\)](#); [Ou et al. \(2025\)](#); [Shi et al. \(2025\)](#)) are a class of MGMs for language modeling that achieve validation perplexity and text quality approaching ARMs. Analogously to continuous diffusion ([Sohl-Dickstein et al., 2015](#); [Song & Ermon, 2020](#); [Ho et al., 2020](#); [Kingma et al., 2023](#)), MDLM defines a fixed corruption process (the *forward process*) and a *generative process* (or reverse process) that recovers clean samples from noise. Formally, the *forward process* is defined as

$$q(\mathbf{z}_t | \mathbf{x}) := \text{Cat}(\mathbf{z}_t; \alpha_t \mathbf{x} + (1 - \alpha_t) \boldsymbol{\pi}), \quad (2)$$

where \mathbf{x} is the one-hot representation of $x \in \mathcal{X}$, and $\boldsymbol{\pi} = \mathbf{m}$ is the one-hot encoding of the **[MASK]** token. The noise schedule $(\alpha_t)_{t=0}^{t=1}$ represents the probability of *not* being masked at time t , and is strictly decreasing with boundary conditions $\alpha_0 = 1, \alpha_1 = 0$. (2) is extended to sequences by

being applied independently at every position. Let $p(\mathbf{z}_s | \mathbf{z}_t, \mathbf{x}) = \frac{p(\mathbf{z}_s | \mathbf{x})p(\mathbf{z}_t | \mathbf{z}_s)}{p(\mathbf{z}_t | \mathbf{x})}$ denote the posterior distribution:

$$p(\mathbf{z}_s | \mathbf{z}_t, \mathbf{x}) = \begin{cases} \text{Cat}(\mathbf{z}_s; \mathbf{z}_t), & \mathbf{z}_t \neq \mathbf{m}, \\ \text{Cat}\left(\mathbf{z}_s; \frac{(1-\alpha_s)\mathbf{m} + (\alpha_s - \alpha_t)\mathbf{x}}{(1-\alpha_t)}\right), & \mathbf{z}_t = \mathbf{m}. \end{cases} \quad (3)$$

The generative process p_θ is chosen to have the same form as (3), only replacing \mathbf{x} , unavailable during sampling, by a denoiser $\mathbf{x}_\theta : \mathcal{X}^L \rightarrow \mathbb{R}^{L \times N}$. That is, $p_\theta(\mathbf{z}_s | \mathbf{z}_t) = p(\mathbf{z}_s | \mathbf{z}_t, \mathbf{x} = \mathbf{x}_\theta)$.

Objective MDLM optimizes a variational bound to the log-likelihood that reduces to a weighted cross-entropy over noise levels, with the same form as in (1), with $w(t) = \frac{\alpha'_t}{1-\alpha_t}$. At unmasked positions, the denoiser simply carries over its input, so only masked positions contribute to the loss.

2.4 MASKGIT

MaskGIT (Chang et al., 2022) is an MGM for image generation that operates on discrete tokens obtained from a pre-trained VQGAN (Esser et al., 2021). Like other MGMs, MaskGIT is trained with the objective in (1). To generate tokens, MaskGIT samples from the predictions of the denoiser \mathbf{x}_θ at all masked positions ℓ . Let $\tilde{x}_\ell \sim \mathbf{x}_\theta(\mathbf{z}_t; t)_{\ell,:}$ denote the value sampled at position ℓ . Let $c_\ell = \mathbf{x}_\theta(\mathbf{z}_t; t)_{\ell, \tilde{x}_\ell}$ denote the probability of the token generated at position ℓ . At each iteration, MaskGIT remarks the tokens with the lowest confidence (over the sequence length). The tokens denoised during previous sampling steps use a confidence of 1, hence are never remasked.

2.5 CLASSIFIER-FREE GUIDANCE

Let $p_\theta(\mathbf{x}|c)$ denote a class-conditional distribution learned via a diffusion, or masked generative model, where $c \in \{0, \dots, N-1\} \cup \{\emptyset\}$, and $p_\theta(\mathbf{x}|\emptyset)$ denotes the class-unconditional distribution. Classifier-free guidance (CFG; Ho & Salimans (2022); Chang et al. (2022)) implements a mechanism with hyperparameter $\omega \geq 1$, to increase the likelihood of samples from a class c during sampling. For MGMs, Chang et al. (2022) implements CFG by replacing the log probabilities $\log p_\theta(\mathbf{x}|c)$ by

$$v_\theta = (1 + \omega) \log p_\theta(\mathbf{x}|c) - \omega \log p_\theta(\mathbf{x}|\emptyset). \quad (4)$$

2.6 SELF-DISTILLATION THROUGH TIME

Self-Distillation Through Time (SDTT) (Deschenaux & Gulcehre, 2025) accelerates sampling from MGMs by training a student MGM whose one-step predictions match the two-step predictions of the original, teacher MGM. Upon convergence, two steps of the student correspond to four steps of the original MGM. Additional distillation rounds that use the trained student as teacher can further reduce the number of sampling steps (Salimans & Ho, 2022).

3 PARTITION GENERATIVE MODELING

Partition Generative Models (PGMs) retain the parallel generation capabilities of MGMs while addressing their computational inefficiencies. The key idea is simple: instead of masking tokens, we partition them into two disjoint groups and constrain the architecture, so that information cannot flow between the groups. This enables processing only the clean tokens during sampling, while learning from all positions during training. We denote the partition using indices 0 and 1, and assume that partition 0 in PGM corresponds to the clean tokens in MGMs and that partition 1 correspond to the masked positions.

Partitioning Let $\mathbf{x} \in \mathcal{D}$ denote a training sequence, and sample $t \sim \mathcal{U}[0, 1]$. While MGMs mask each token with probability p_t (e.g., $p_t = 1 - \alpha_t$ for MDLM), PGMs instead assign each token to group 1 with probability p_t , and to group 0 otherwise. Let $\mathbf{g} \in \{0, 1\}^L$ denote the binary vector indicating group membership for each position.

Training objective PGMs are trained with an objective similar to (1), but apply separate weighting functions to each partition group, to account for their relative sizes. Let p_t be the probability of

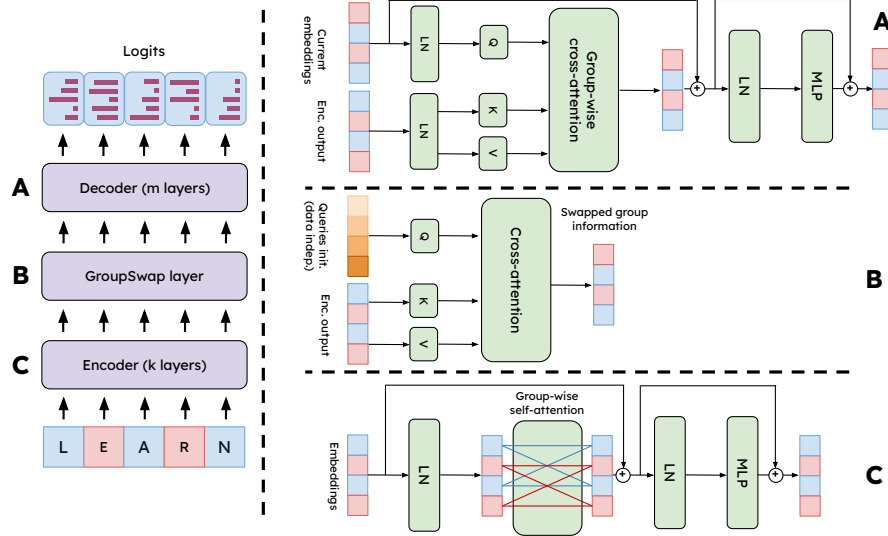


Figure 3: **PGM-compatible transformer architecture.** RoPE (Su et al., 2023) is applied before every attention layer but not shown for clarity. (A) Decoder layer with cross-attention to the encoder output and no self-attention between tokens. (B) GroupSwap layer that exchanges information between positions in group 0 and group 1, enabling each group to make predictions based on tokens from the other group. (C) Encoder layer with sparse, group-wise self-attention.

assigning a token to group 1. Then, group 1 predicts a fraction $1 - p_t$ of the tokens, while group 0 predicts a fraction p_t . To remain consistent with the MGM objective, tokens in group 0 use a weight $w(t)$, since they have access to the same information as an MGM at time t . Therefore, the training objective for PGMs is

$$\mathcal{L}_{\text{PGM}} := \mathbb{E}_{\mathbf{x} \sim \mathcal{D}, t \sim \mathcal{U}[0,1]} \left[w^{\text{PGM}}(\mathbf{g}, t) \text{CE}(\mathbf{x}_\theta(\mathbf{x}; \mathbf{g}; t), \mathbf{x}) \right], \quad (5)$$

where

$$w^{\text{PGM}}(\mathbf{g}, t)_i = \begin{cases} w(t) & \text{if } \mathbf{g}_i = 0 \\ w(1 - t) & \text{if } \mathbf{g}_i = 1. \end{cases} \quad (6)$$

Figure 2a (left) shows that in a single forward pass of an MGM, the loss is computed for the masked positions only. In contrast, as shown in Figure 2b (left), PGMs compute a loss at every position. Although the task in (5) may appear trivial, since the model is trained to predict its input, we design the architecture (Sec. 4) so that the predictions for tokens in group 1 depend on group 0 only, and vice-versa. This mirrors the setup in MGMs, where a fraction of the positions is masked and must be predicted from the clean tokens. Since the denoiser learns to predict each group conditioned on the other, within a single sequence, each sequence effectively contains two sub-training-examples. Conceptually, *this is equivalent to training on two complementary masked sequences in the same batch*.

Sampling Because tokens in different groups do not interact, PGMs, like ARMs, process only the clean tokens during inference, rather than carrying numerous [MASK] tokens as MGMs (Figure 2b, right). Unlike ARMs, which predict a single token at a time, PGMs output categorical distributions for $k \geq 1$ positions simultaneously. This allows PGMs to preserve the parallel and flexible sampling of MGMs, while, like ARMs, predicting only the tokens that will actually be decoded. Assuming the same posterior $p_\theta(\mathbf{z}_s \mid \mathbf{z}_t)$ as MDLM in (3), a PGM denoises each [MASK] token independently with probability $\frac{\alpha_s - \alpha_t}{1 - \alpha_t}$. Equivalently, the number of denoised positions can be viewed as drawn from a Binomial $\left(L, \frac{\alpha_s - \alpha_t}{1 - \alpha_t}\right)$ distribution. In practice, one may denoise a fixed number of tokens per batch for simplicity (Algo. 1), or allow a variable number per example by using padding (Algo. 2).

Model ↓	#Params	Val. PPL	Latency (sec) ↓	TP (tok/sec) ↑
<i>LM1B (ctx len. 128)</i>				
MDLM	170M	27.67	3.78	1'081.57
MDLM [†] (Compl. masking)	170M	25.72	3.78	1'081.57
PGM 6 / 6	171M	<u>26.80</u>	2.12	1'930.93
<i>OpenWebText (ctx len. 1024)</i>				
MDLM	170M	23.07	31.41	1'043.22
MDLM [†] (Compl. masking)	170M	22.98	31.41	1'043.22
PGM 8 / 8	203M	<u>22.61</u>	5.86	5'585.57
PGM 6 / 6 (dim. 1024)	268M	21.43	5.93	5'518.09

Table 1: **Validation Perplexity:** On LM1B, PGM with matching number of layers outperform MDLM. $PGM\ k / m$ denotes our model with k encoder and m decoder layers. We highlight the best PGM in gray. The sampling latency and throughput (TP) are measured with a batch size of 32. **On OWT, our PGM outperforms MDLM while delivering at least 5× higher throughput.** See Table 5 for ablations on the architecture. [†] Models trained with a 2× larger batch size (Sec. 5.3).

4 THE PARTITION TRANSFORMER

As discussed in Sec. 3, PGMs are trained to predict their own input. This task is only non-trivial if the architecture prevents information flow across the groups of the partition. Consequently, standard bidirectional transformers are not suited. To address this, we propose the *Partition Transformer*, a dedicated architecture for implementing PGMs, illustrated in Figure 3. The architecture consists of three components: an encoder, a *GroupSwap* layer, and a decoder.

Encoder The encoder is made of partition-wise self-attention blocks, which are similar to standard bidirectional transformer blocks except that tokens in separate groups do not attend to each other.

Decoder The decoder uses cross-attention layers, whose keys and values are computed based on the output of the encoder. In contrast, the queries are computed using either the output of the *GroupSwap* layer (for the first block of the decoder) or the output of the previous decoder block. Importantly, *there is no self-attention layer in the decoder*, which allows efficient generation, as we can compute predictions solely at the positions that we will decode.

4.1 THE GROUPSWAP LAYER

In the encoder, information remains localized: if a token belongs to group 0, its hidden representation only depend on tokens in group 0. For prediction, however, we require the opposite: representations at positions in group 0 must depend exclusively on group 1, and vice versa. To enforce this, we introduce the *GroupSwap* layer (Figure 3B), which exchanges information between groups. The *GroupSwap* layer is implemented using cross-attention. If a token at position ℓ belongs to group 0, the predictions at position ℓ must rely only on information from group 1. Hence, to prevent information leakage, the queries used in cross-attention cannot depend on tokens in group 0. We describe two ways of initializing these queries below.

Data-Independent Queries Let $\mathbf{u} \in \mathbb{R}^H$ be a learnable vector. To initialize the queries, we replicate \mathbf{u} across the sequence length, add fixed positional encodings, and apply layer normalization followed by a linear projection. Formally, let $V \in \mathbb{R}^{L \times H}$ denote the initialized query matrix, with $V_{i,:}$ the i -th row. Then

$$V_{i,:} = W \left[\text{LN} \left(\mathbf{u} + \text{pos}_{i,:} \right) + b \right], \quad (7)$$

where $W \in \mathbb{R}^{H \times H}$, $b \in \mathbb{R}^H$ are learnable parameters and LN denotes layer normalization (Ba et al., 2016). We use sinusoidal positional encoding (Vaswani et al., 2023):

$$\text{pos}_{i,j} = \begin{cases} \cos \left(\frac{i}{10000^{2j/H}} \right) & \text{if } j < H/2 \\ \sin \left(\frac{i}{10000^{2j/H-1}} \right) & \text{otherwise} \end{cases} \quad (8)$$

Data-Dependent Queries Let $X \in \mathbb{R}^{L \times H}$ be the encoder output. We first perform a group-wise aggregation over the sequence length (e.g., `logsumexp` or `mean`) to obtain vectors $Y_0, Y_1 \in \mathbb{R}^H$, representing the aggregated information for groups 0 and 1, respectively. The data-dependent query initialization V' is then computed as

$$V'_{i,:} = V_{i,:} + \begin{cases} Y_1, & \text{if } g_i = 0 \\ Y_0 & \text{otherwise.} \end{cases} \quad (9)$$

5 EXPERIMENTS

We compare PGM with MDLM (Sahoo et al., 2024) on standard language modeling datasets, training on LM1B (Chelba et al., 2014) and OpenWebText (OWT; Gokaslan & Cohen (2019)) in Sec. 5.1. We evaluate them using the validation perplexity and downstream task accuracy before and after distillation with SDTT (Deschenaux & Gulcehre, 2025). We compare PGM with MaskGIT (Chang et al., 2022) on VQGAN-quantized (Esser et al., 2021) ImageNet256 (Deng et al., 2009) (Sec. 5.2). As described in Sec. 3, by predicting each group from the other, PGMs implement a mechanism akin to training on two complementary masked sequences per batch, while also introducing a new architecture (Sec. 4). The effect of complementary masking is studied in isolation in Sec. 5.3. Our experiments show that, for both language and image modeling, and after distillation, PGMs are competitive with MDLM and MaskGIT, while **providing a $5\text{--}5.5\times$ throughput improvement for text and a $7.5\times$ improvement for images**. Find more experimental details in Suppl. C.

5.1 LANGUAGE MODELING

Experimental settings We closely follow the settings of Sahoo et al. (2024). MDLM uses a modified Diffusion Transformer (Peebles & Xie, 2023; Lou et al., 2024) with RoPE (Su et al., 2023), with 12 layers and an embedding dimension of 768, without time conditioning. We train with a global batch size of 512 for 1M steps, dropout of 0.1, and the Adam optimizer with learning rate 3×10^{-4} and no weight decay. We maintain and Exponential Moving Average (EMA) of the weights with decay 0.9999. For PGM, we use the Partition Transformer architecture (Sec. 4) with 12 or 16 layers, embedding dimensions of 768 or 1024, and varying numbers of encoder and decoder layers. On LM1B, all models use a context length of 128, with shorter documents padded and tokenized using the `bert-base-uncased` (Devlin et al., 2019) tokenizer. On OWT, we use a context length of 1024 with sentence packing (Raffel et al., 2023) with the GPT-2 tokenizer and insert an [EOS] token between documents. Since the dataset lacks an official validation split, the last 100k documents are reserved for validation. To evaluate the sample quality, we use the Generative Perplexity (Gen. PPL), computed using GPT-2 Large (Radford et al., 2019), following Sahoo et al. (2024). We cast the logits in `float64` prior to sampling, following Zheng et al. (2025).

Likelihood Evaluation After 1M steps, PGMs with as many layers as MDLM achieve a **validation perplexity of 1.95 lower than MDLM on LM1B** (Table 1). Table 5 (left) shows that balanced models with equal numbers of encoder and decoder layers outperform imbalanced variants. Interestingly, data-independent queries perform comparably to data-dependent queries, so we use the simpler, data-independent version in all subsequent experiments. On OpenWebText, PGMs with the same number of layers and embedding dimension as MDLM slightly underperform (Table 5, right). Increasing the number of encoder and decoder layers by two, or increasing the embedding dimension to 1024, allows PGMs to surpass MDLM in validation perplexity, while **achieving at least $5\times$ higher sampling throughput**. This improved efficiency makes PGMs particularly attractive for scaling test-time computation (Madaan et al., 2023; Yao et al., 2023; Snell et al., 2024; Wu et al., 2024; Chen et al., 2024; Brown et al., 2024; Goyal et al., 2024).

Downstream Evaluation Following Deschenaux & Gulcehre (2024); Nie et al. (2025), we evaluate MDLM and PGMs trained on OpenWebText using the `lm-eval-harness` suite (Gao et al., 2024). As shown in Table 2, PGMs slightly outperform MDLM on six out of eight tasks, although the overall accuracy across models is similar. This suggests that **PGM achieves faster inference without sacrificing downstream performance**. Since `lm-eval-harness` is originally designed for ARMs, we must adapt it for MPMs. Fortunately, both MDLM and PGM can compute a variational

bound on the likelihood, which is used in place of the true likelihood to select the most probable answer in multiple-choice tasks. Additional details and tasks are provided in Suppl. D.5.

Distillation of PGMs After likelihood training, PGMs achieve $5 - 5.5 \times$ higher throughput than MDLM. To further accelerate sampling, we apply Self-Distillation Through Time (SDTT; Deschenaux & Gulcehre (2025)). To remain as faithful as possible to the implementation of Deschenaux & Gulcehre (2025), we apply the distillation loss to a single group while treating the other as [MASK] tokens. This shows that PGMs are compatible with distillation methods designed for MGMs. We leave the development of new distillation strategies for PGMs to future work. Hence, the setup naturally favors MDLM. Figure 4 (right) and Table 6 compare the Gen. PPL, unigram entropy, and sampling speed of PGM and MDLM. After five rounds of distillation, and with standard ancestral sampling, PGMs achieve higher Generative Perplexity and entropy than MDLM. With nucleus sampling ($p = 0.9$) (Holtzman et al., 2020), PGMs produce samples with comparable perplexity and entropy. Due to the overhead of nucleus sampling, the speed advantage of PGMs decreases from at least $5 \times$ to approximately $4.6 \times$ faster than MDLM for the same number of steps (Fig. 4). Generative perplexity alone does not fully capture language model performance, hence we also evaluate distilled models on downstream tasks. As shown in Table 2, distillation slightly shifts accuracy across tasks, but overall performance remains similar. **PGMs still achieve slightly higher accuracy than MDLM on most tasks after distillation.**

5.2 IMAGE MODELING

Experimental Settings We train MaskGIT (Chang et al., 2022) and PGM on ImageNet256. Images are cropped to a centered square along the longer side and then rescaled to 256×256 . We use the MaskGIT implementation of Besnier et al. (2025), including their pre-trained VQ-GAN tokenizer. We train for 500k steps with a batch size of 256 using AdamW (weight decay 0.03, learning rate $1e-4$, cosine schedule with 2500 warmup steps). We use a dropout of 0.1 in the Transformer. All models are class-conditional, with a class-label dropout of 0.1 to enable classifier-free guidance (CFG) at sampling time. As Besnier et al. (2025), we train with one register (Dariset et al., 2024) for the MaskGIT baseline, and two (one per group) for PGM, so that we can use one register during sampling.

Results In Figure 1 (left), we compare the Fréchet Inception Distance (FID; Heusel et al. (2018)) of samples from MaskGIT (Chang et al., 2022) and PGM, using the Halton sampler and classifier-free guidance with the guidance weight $w \in \{0, 1, \dots, 6\}$ that yields the lowest FID. PGM 12/12 achieves a $7.5 \times$ higher throughput with only a slight FID degradation (5.54 vs. 5.35). **Increasing the sampling steps to 64 further improves the FID to 4.56, while remaining $3.9 \times$ faster than MaskGIT.** See Suppl. D.3 for full results across guidance strengths.

5.3 ISOLATING THE EFFECT OF COMPLEMENTARY MASKING

Experimental Setup To disentangle the contributions of PGM, we isolate the effect of complementary masking (Sec. 3) by training a standard bidirectional Transformer with double the batch size. Each input sequence is turned into two complementary masked copies: if the token at position ℓ is masked in one copy, it remains unmasked in the other. This setup provides an upper bound on the potential gains, as it directly measures the benefit of complementary masks during training.

Results Table 1 shows that complementary masking improves the validation perplexity on LM1B and OWT, though with smaller gains on OWT. On both datasets, a gap remains between PGM and MDLM with complementary masking. This suggests that the current neural network architecture can be improved further. Because of the smaller improvement on OWT, we must increase the parameter

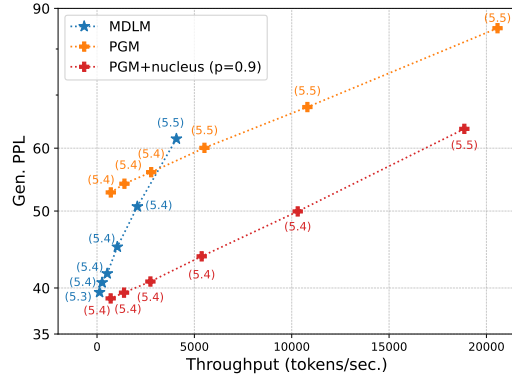


Figure 4: After distillation, PGM (6 / 6, dim. 1024) with nucleus sampling remains significantly faster than MDLM, at matching entropy and Gen. PPL.

We sample with the confidence and Halton samplers.

Figure 4: After distillation, PGM (6 / 6, dim. 1024) with nucleus sampling remains significantly faster than MDLM, at matching entropy and Gen. PPL.

We sample with the confidence and Halton samplers.

Table 2: **Accuracy on downstream tasks** (Gao et al., 2024). HS: HellaSwag, OQA: OpenBook QA. Arc: Arc-easy. We select the tasks following Nie et al. (2025). We see that distillation slightly changes the downstream tasks performance, but that PGMs continue to outperform MDLM on most tasks. The best performance is **bolded**, while the second best is underlined.

	LAMBADA	Arc	BoolQ	HS	OQA	PIQA	RACE	SIQA
<i>Before Distillation</i>								
MDLM	38.52	37.88	49.42	31.36	28.60	58.27	28.04	38.84
PGM 8 / 8	46.98	40.40	53.49	<u>33.20</u>	<u>26.60</u>	<u>58.92</u>	26.89	<u>39.97</u>
PGM 6 / 6 (1024)	<u>41.39</u>	<u>39.98</u>	<u>49.82</u>	34.27	25.40	59.19	<u>27.37</u>	40.28
<i>After Distillation (SDTT)</i>								
MDLM	41.34	33.80	48.59	30.75	28.80	57.73	27.94	38.79
PGM 8 / 8	47.22	37.42	51.50	<u>31.62</u>	<u>25.80</u>	<u>59.03</u>	30.62	39.61
PGM 6 / 6 (1024)	<u>44.48</u>	<u>36.70</u>	<u>49.36</u>	32.55	25.00	59.85	27.37	<u>39.25</u>

count to surpass MDLM. Nonetheless, recall that despite having more parameters, PGMs remain at least $5\times$ faster than MDLM during sampling. In Suppl. D.1, we present preliminary experiments exploring why complementary masking improves performance on LM1B but not on OpenWebText.

6 RELATED WORK

Discrete Diffusion Although autoregressive models currently dominate text generation, recent advances in discrete diffusion (Austin et al., 2023; Lou et al., 2024; Shi et al., 2025; Sahoo et al., 2024; von Rütte et al., 2025; Schiff et al., 2025; Haxholli et al., 2025; Sahoo et al., 2025a) and discrete flow matching (Campbell et al., 2024; Gat et al., 2024) have demonstrated that MCMs can approach AR models in generation quality. We propose an efficient inference approach that does not require processing [MASK] tokens but does not require changing the modeling framework.

Variable Length Masked Diffusion Block Diffusion (BD; Arriola et al. (2025)) interpolates between ARMs and MDLMs, enabling parallelism and partial KV-caching (Pope et al., 2022), but generates tokens in a (block-)autoregressive way. In contrast, PGMs permit arbitrary generation orders. Extensions of MCMs include flexible-length generation via stochastic interpolants (Kim et al., 2025; Albergo et al., 2023) and edit operations through discrete flow matching (Havasi et al., 2025; Gat et al., 2024). Sahoo et al. (2025b) pursue a related hybrid of autoregressive and masked diffusion, though by a different route (see Suppl. B for details). PGMs are mostly orthogonal to these efforts: we remain compatible with such frameworks as we focus on preserving the original objective while focusing on the architecture.

Non-Autoregressive Language Models Any-order and any-subset autoregressive models (Yang et al., 2020; Pannatier et al., 2024; Shih et al., 2022; Guo & Ermon, 2025) learn an autoregressive distribution of tokens given arbitrary token subsets. In contrast, in this work, we accelerate MDLMs, which do not enforce causal attention on the tokens.

7 CONCLUSION

We introduce Partition Generative Modeling (PGM), a novel approach to masked generative modeling that eliminates [MASK] tokens entirely. PGM achieves significant improvements in inference speed on both text and images, with minimal effect on quality. The significant improvements suggest that PGM might be suited for domains that benefit from test-time scaling, such as coding and reasoning. We show that PGMs can be distilled for further acceleration. Future work could explore optimizations to the PGM architecture, investigating distillation techniques specifically designed for PGMs, and extending the approach to multimodal settings. In summary, PGM offers an alternative to masked generative models, with particular advantages for applications where inference speed is critical.

8 ACKNOWLEDGEMENTS

This work has received funding from the Swiss State Secretariat for Education, Research and Innovation (SERI). We are grateful to Razvan Pascanu for insightful discussions. We acknowledge the SCITAS team at EPFL for providing access to their cluster, and the Swiss National Supercomputing Centre for the Alps platform. We are grateful to Karin Gétaz for her administrative assistance.

REFERENCES

Michael S. Albergo, Nicholas M. Boffi, and Eric Vanden-Eijnden. Stochastic interpolants: A unifying framework for flows and diffusions, 2023. URL <https://arxiv.org/abs/2303.08797>.

Marianne Arriola, Aaron Gokaslan, Justin T Chiu, Zhihan Yang, Zhixuan Qi, Jiaqi Han, Subham Sekhar Sahoo, and Volodymyr Kuleshov. Block diffusion: Interpolating between autoregressive and diffusion language models, 2025. URL <https://arxiv.org/abs/2503.09573>.

Jacob Austin, Daniel D. Johnson, Jonathan Ho, Daniel Tarlow, and Rianne van den Berg. Structured denoising diffusion models in discrete state-spaces, 2023. URL <https://arxiv.org/abs/2107.03006>.

Jimmy Lei Ba, Jamie Ryan Kiros, and Geoffrey E. Hinton. Layer normalization, 2016. URL <https://arxiv.org/abs/1607.06450>.

Victor Besnier, Mickael Chen, David Hurich, Eduardo Valle, and Matthieu Cord. Halton scheduler for masked generative image transformer, 2025. URL <https://arxiv.org/abs/2503.17076>.

Bradley Brown, Jordan Juravsky, Ryan Ehrlich, Ronald Clark, Quoc V. Le, Christopher Ré, and Azalia Mirhoseini. Large language monkeys: Scaling inference compute with repeated sampling, 2024. URL <https://arxiv.org/abs/2407.21787>.

Andrew Campbell, Joe Benton, Valentin De Bortoli, Tom Rainforth, George Deligiannidis, and Arnaud Doucet. A continuous time framework for discrete denoising models, 2022. URL <https://arxiv.org/abs/2205.14987>.

Andrew Campbell, Jason Yim, Regina Barzilay, Tom Rainforth, and Tommi Jaakkola. Generative flows on discrete state-spaces: Enabling multimodal flows with applications to protein co-design, 2024. URL <https://arxiv.org/abs/2402.04997>.

Huiwen Chang, Han Zhang, Lu Jiang, Ce Liu, and William T. Freeman. Maskgit: Masked generative image transformer, 2022. URL <https://arxiv.org/abs/2202.04200>.

Ciprian Chelba, Tomas Mikolov, Mike Schuster, Qi Ge, Thorsten Brants, Philipp Koehn, and Tony Robinson. One billion word benchmark for measuring progress in statistical language modeling, 2014. URL <https://arxiv.org/abs/1312.3005>.

Lingjiao Chen, Jared Quincy Davis, Boris Hanin, Peter Bailis, Ion Stoica, Matei Zaharia, and James Zou. Are more llm calls all you need? towards scaling laws of compound inference systems, 2024. URL <https://arxiv.org/abs/2403.02419>.

Marco Comunità, Zhi Zhong, Akira Takahashi, Shiqi Yang, Mengjie Zhao, Koichi Saito, Yukara Ikemiya, Takashi Shibuya, Shusuke Takahashi, and Yuki Mitsufuji. Specmaskgit: Masked generative modeling of audio spectrograms for efficient audio synthesis and beyond, 2024. URL <https://arxiv.org/abs/2406.17672>.

Timothée Dariset, Maxime Oquab, Julien Mairal, and Piotr Bojanowski. Vision transformers need registers, 2024. URL <https://arxiv.org/abs/2309.16588>.

Jia Deng, Wei Dong, Richard Socher, Li-Jia Li, Kai Li, and Li Fei-Fei. Imagenet: A large-scale hierarchical image database. In *2009 IEEE conference on computer vision and pattern recognition*, pp. 248–255. Ieee, 2009.

Justin Deschenaux and Caglar Gulcehre. Promises, outlooks and challenges of diffusion language modeling, 2024. URL <https://arxiv.org/abs/2406.11473>.

Justin Deschenaux and Caglar Gulcehre. Beyond autoregression: Fast llms via self-distillation through time, 2025. URL <https://arxiv.org/abs/2410.21035>.

Jacob Devlin, Ming-Wei Chang, Kenton Lee, and Kristina Toutanova. Bert: Pre-training of deep bidirectional transformers for language understanding, 2019. URL <https://arxiv.org/abs/1810.04805>.

Sander Dieleman, Laurent Sartran, Arman Roshannai, Nikolay Savinov, Yaroslav Ganin, Pierre H. Richemond, Arnaud Doucet, Robin Strudel, Chris Dyer, Conor Durkan, Curtis Hawthorne, Rémi Leblond, Will Grathwohl, and Jonas Adler. Continuous diffusion for categorical data, 2022. URL <https://arxiv.org/abs/2211.15089>.

Juechu Dong, Boyuan Feng, Driss Guessous, Yanbo Liang, and Horace He. Flex attention: A programming model for generating optimized attention kernels, 2024. URL <https://arxiv.org/abs/2412.05496>.

Patrick Esser, Robin Rombach, and Björn Ommer. Taming transformers for high-resolution image synthesis, 2021. URL <https://arxiv.org/abs/2012.09841>.

Rohit Gandikota and David Bau. Distilling diversity and control in diffusion models, 2025. URL <https://arxiv.org/abs/2503.10637>.

Leo Gao, Jonathan Tow, Baber Abbasi, Stella Biderman, Sid Black, Anthony DiPofi, Charles Foster, Laurence Golding, Jeffrey Hsu, Alain Le Noac'h, Haonan Li, Kyle McDonell, Niklas Muennighoff, Chris Ociepa, Jason Phang, Laria Reynolds, Hailey Schoelkopf, Aviya Skowron, Lintang Sutawika, Eric Tang, Anish Thite, Ben Wang, Kevin Wang, and Andy Zou. The language model evaluation harness, 07 2024. URL <https://zenodo.org/records/12608602>.

Itai Gat, Tal Remez, Neta Shaul, Felix Kreuk, Ricky T. Q. Chen, Gabriel Synnaeve, Yossi Adi, and Yaron Lipman. Discrete flow matching, 2024. URL <https://arxiv.org/abs/2407.15595>.

Aaron Gokaslan and Vanya Cohen. Openwebtext corpus. <http://Skylion007.github.io/OpenWebTextCorpus>, 2019.

Sachin Goyal, Ziwei Ji, Ankit Singh Rawat, Aditya Krishna Menon, Sanjiv Kumar, and Vaishnavh Nagarajan. Think before you speak: Training language models with pause tokens, 2024. URL <https://arxiv.org/abs/2310.02226>.

Gabe Guo and Stefano Ermon. Reviving any-subset autoregressive models with principled parallel sampling and speculative decoding, 2025. URL <https://arxiv.org/abs/2504.20456>.

Marton Havasi, Brian Karrer, Itai Gat, and Ricky T. Q. Chen. Edit flows: Flow matching with edit operations, 2025. URL <https://arxiv.org/abs/2506.09018>.

Etrit Haxholli, Yeti Z. Gurbuz, Oğul Can, and Eli Waxman. Efficient perplexity bound and ratio matching in discrete diffusion language models. In *The Thirteenth International Conference on Learning Representations*, 2025. URL <https://openreview.net/forum?id=Mri9WIfxSm>.

Satoshi Hayakawa, Yuhta Takida, Masaaki Imaizumi, Hiromi Wakaki, and Yuki Mitsuji. Distillation of discrete diffusion through dimensional correlations, 2025. URL <https://arxiv.org/abs/2410.08709>.

Martin Heusel, Hubert Ramsauer, Thomas Unterthiner, Bernhard Nessler, and Sepp Hochreiter. Gans trained by a two time-scale update rule converge to a local nash equilibrium, 2018. URL <https://arxiv.org/abs/1706.08500>.

Jonathan Ho and Tim Salimans. Classifier-free diffusion guidance, 2022. URL <https://arxiv.org/abs/2207.12598>.

Jonathan Ho, Ajay Jain, and Pieter Abbeel. Denoising diffusion probabilistic models, 2020. URL <https://arxiv.org/abs/2006.11239>.

Ari Holtzman, Jan Buys, Li Du, Maxwell Forbes, and Yejin Choi. The curious case of neural text degeneration, 2020. URL <https://arxiv.org/abs/1904.09751>.

Jaeyeon Kim, Lee Cheuk-Kit, Carles Domingo-Enrich, Yilun Du, Sham Kakade, Timothy Ngotiaoco, Sitan Chen, and Michael Albergo. Any-order flexible length masked diffusion, 2025. URL <https://arxiv.org/abs/2509.01025>.

Diederik P. Kingma and Jimmy Ba. Adam: A method for stochastic optimization, 2017. URL <https://arxiv.org/abs/1412.6980>.

Diederik P. Kingma, Tim Salimans, Ben Poole, and Jonathan Ho. Variational diffusion models, 2023. URL <https://arxiv.org/abs/2107.00630>.

Aaron Lou, Chenlin Meng, and Stefano Ermon. Discrete diffusion modeling by estimating the ratios of the data distribution, 2024. URL <https://arxiv.org/abs/2310.16834>.

Aman Madaan, Niket Tandon, Prakhar Gupta, Skyler Hallinan, Luyu Gao, Sarah Wiegreffe, Uri Alon, Nouha Dziri, Shrimai Prabhumoye, Yiming Yang, Shashank Gupta, Bodhisattwa Prasad Majumder, Katherine Hermann, Sean Welleck, Amir Yazdanbakhsh, and Peter Clark. Self-refine: Iterative refinement with self-feedback, 2023. URL <https://arxiv.org/abs/2303.17651>.

Shen Nie, Fengqi Zhu, Chao Du, Tianyu Pang, Qian Liu, Guangtao Zeng, Min Lin, and Chongxuan Li. Scaling up masked diffusion models on text, 2025. URL <https://arxiv.org/abs/2410.18514>.

Jingyang Ou, Shen Nie, Kaiwen Xue, Fengqi Zhu, Jiacheng Sun, Zhenguo Li, and Chongxuan Li. Your absorbing discrete diffusion secretly models the conditional distributions of clean data, 2025. URL <https://arxiv.org/abs/2406.03736>.

Arnaud Pannatier, Evann Courdier, and François Fleuret. Sigma-gpts: A new approach to autoregressive models, 2024. URL <https://arxiv.org/abs/2404.09562>.

William Peebles and Saining Xie. Scalable diffusion models with transformers, 2023. URL <https://arxiv.org/abs/2212.09748>.

Reiner Pope, Sholto Douglas, Aakanksha Chowdhery, Jacob Devlin, James Bradbury, Anselm Levskaya, Jonathan Heek, Kefan Xiao, Shivani Agrawal, and Jeff Dean. Efficiently scaling transformer inference, 2022. URL <https://arxiv.org/abs/2211.05102>.

Alec Radford, Jeffrey Wu, Rewon Child, David Luan, Dario Amodei, Ilya Sutskever, et al. Language models are unsupervised multitask learners. *OpenAI blog*, 1(8):9, 2019.

Colin Raffel, Noam Shazeer, Adam Roberts, Katherine Lee, Sharan Narang, Michael Matena, Yanqi Zhou, Wei Li, and Peter J. Liu. Exploring the limits of transfer learning with a unified text-to-text transformer, 2023. URL <https://arxiv.org/abs/1910.10683>.

Subham Sekhar Sahoo, Marianne Arriola, Yair Schiff, Aaron Gokaslan, Edgar Marroquin, Justin T Chiu, Alexander Rush, and Volodymyr Kuleshov. Simple and effective masked diffusion language models, 2024. URL <https://arxiv.org/abs/2406.07524>.

Subham Sekhar Sahoo, Justin Deschenaux, Aaron Gokaslan, Guanghan Wang, Justin Chiu, and Volodymyr Kuleshov. The diffusion duality, 2025a. URL <https://arxiv.org/abs/2506.10892>.

Subham Sekhar Sahoo, Zhihan Yang, Yash Akhauri, Johnna Liu, Deepansha Singh, Zhoujun Cheng, Zhengzhong Liu, Eric Xing, John Thickstun, and Arash Vahdat. Esoteric language models, 2025b. URL <https://arxiv.org/abs/2506.01928>.

Tim Salimans and Jonathan Ho. Progressive distillation for fast sampling of diffusion models, 2022. URL <https://arxiv.org/abs/2202.00512>.

Tim Salimans, Ian Goodfellow, Wojciech Zaremba, Vicki Cheung, Alec Radford, and Xi Chen. Improved techniques for training gans, 2016. URL <https://arxiv.org/abs/1606.03498>.

Yair Schiff, Subham Sekhar Sahoo, Hao Phung, Guanghan Wang, Sam Boshar, Hugo Dalla-torre, Bernardo P. de Almeida, Alexander Rush, Thomas Pierrot, and Volodymyr Kuleshov. Simple guidance mechanisms for discrete diffusion models, 2025. URL <https://arxiv.org/abs/2412.10193>.

Jiaxin Shi, Kehang Han, Zhe Wang, Arnaud Doucet, and Michalis K. Titsias. Simplified and generalized masked diffusion for discrete data, 2025. URL <https://arxiv.org/abs/2406.04329>.

Andy Shih, Dorsa Sadigh, and Stefano Ermon. Training and inference on any-order autoregressive models the right way, 2022. URL <https://arxiv.org/abs/2205.13554>.

Charlie Snell, Jaehoon Lee, Kelvin Xu, and Aviral Kumar. Scaling lilm test-time compute optimally can be more effective than scaling model parameters, 2024. URL <https://arxiv.org/abs/2408.03314>.

Jascha Sohl-Dickstein, Eric Weiss, Niru Maheswaranathan, and Surya Ganguli. Deep unsupervised learning using nonequilibrium thermodynamics. In Francis Bach and David Blei (eds.), *Proceedings of the 32nd International Conference on Machine Learning*, volume 37 of *Proceedings of Machine Learning Research*, pp. 2256–2265, Lille, France, 07–09 Jul 2015. PMLR. URL <https://proceedings.mlr.press/v37/sohl-dickstein15.html>.

Yang Song and Stefano Ermon. Generative modeling by estimating gradients of the data distribution, 2020. URL <https://arxiv.org/abs/1907.05600>.

Jianlin Su, Yu Lu, Shengfeng Pan, Ahmed Murtadha, Bo Wen, and Yunfeng Liu. Roformer: Enhanced transformer with rotary position embedding, 2023. URL <https://arxiv.org/abs/2104.09864>.

Ashish Vaswani, Noam Shazeer, Niki Parmar, Jakob Uszkoreit, Llion Jones, Aidan N. Gomez, Łukasz Kaiser, and Illia Polosukhin. Attention is all you need, 2023. URL <https://arxiv.org/abs/1706.03762>.

Ruben Villegas, Mohammad Babaeizadeh, Pieter-Jan Kindermans, Hernan Moraldo, Han Zhang, Mohammad Taghi Saffar, Santiago Castro, Julius Kunze, and Dumitru Erhan. Phenaki: Variable length video generation from open domain textual description, 2022. URL <https://arxiv.org/abs/2210.02399>.

Dimitri von Rütte, Janis Fluri, Yuhui Ding, Antonio Orvieto, Bernhard Schölkopf, and Thomas Hofmann. Generalized interpolating discrete diffusion, 2025. URL <https://arxiv.org/abs/2503.04482>.

Yangzhen Wu, Zhiqing Sun, Shanda Li, Sean Welleck, and Yiming Yang. An empirical analysis of compute-optimal inference for problem-solving with language models, 2024. URL <https://arxiv.org/abs/2408.00724>.

Zhilin Yang, Zihang Dai, Yiming Yang, Jaime Carbonell, Ruslan Salakhutdinov, and Quoc V. Le. Xlnet: Generalized autoregressive pretraining for language understanding, 2020. URL <https://arxiv.org/abs/1906.08237>.

Shunyu Yao, Dian Yu, Jeffrey Zhao, Izhak Shafran, Thomas L. Griffiths, Yuan Cao, and Karthik Narasimhan. Tree of thoughts: Deliberate problem solving with large language models, 2023. URL <https://arxiv.org/abs/2305.10601>.

Lijun Yu, Yong Cheng, Kihyuk Sohn, José Lezama, Han Zhang, Huiwen Chang, Alexander G. Hauptmann, Ming-Hsuan Yang, Yuan Hao, Irfan Essa, and Lu Jiang. Magvit: Masked generative video transformer, 2023. URL <https://arxiv.org/abs/2212.05199>.

Lingxiao Zhao, Xueying Ding, Lijun Yu, and Leman Akoglu. Unified discrete diffusion for categorical data, 2024. URL <https://arxiv.org/abs/2402.03701>.

Kaiwen Zheng, Yongxin Chen, Hanzi Mao, Ming-Yu Liu, Jun Zhu, and Qinsheng Zhang. Masked diffusion models are secretly time-agnostic masked models and exploit inaccurate categorical sampling, 2025. URL <https://arxiv.org/abs/2409.02908>.

Yuanzhi Zhu, Xi Wang, Stéphane Lathuilière, and Vicky Kalogeiton. Di[M]o: Distilling masked diffusion models into one-step generator, 2025. URL <https://arxiv.org/abs/2503.15457>.

A LIMITATIONS

To match the validation perplexity of the MDLM baseline at a context length of 1024, our models require an increased parameter count. We attribute this to the GroupSwap layer, and future work will explore more efficient mechanisms for information exchange between groups in PGMs. While PGMs offer faster inference, their training is slightly more computationally expensive (Section E), as we use `torch`’s default attention implementation (“`sdpa`”) for simplicity. By reordering tokens according to their group assignment, the self-attention matrices becomes block-diagonal. Future work will explore efficient kernel implementations that exploit this block-diagonal sparsity. Partition Generative Modeling is a general framework, and its application to multimodal settings remains an open direction for future research.

B COMPARISON WITH ESOTERIC LANGUAGE MODELS

Esoteric Language Models (Eso-LMs; [Sahoo et al. \(2025b\)](#)) train hybrid AR-MGM models with a mixture of autoregressive and masked-diffusion objectives, requiring a pre-determined split of training examples between the two modes. In contrast, our method retains the standard MGM objective, differing only by a reweighting of the loss across partition groups, and thus introduces no additional hyperparameters.

Like PGMs, Eso-LMs support any-order generation and thus require custom attention patterns, which may slow training; they mitigate this with FlexAttention ([Dong et al., 2024](#)), which should also be compatible with our approach. At sampling time, Eso-LMs combine a diffusion phase with sequential decoding, where KV-caching is enabled via causal masking. While PGMs do not impose causal attention, they should remain compatible with causal masking, and can incorporate KV-caching-based speedups if desired, though our reported gains do not rely on it.

During training, Eso-LMs still rely on [MASK] tokens, whereas PGMs do not, thanks to our partitioned architecture. This provides denser supervision, which appears beneficial for shorter sequences.

C EXPERIMENTAL DETAILS

We trained all models from scratch. Our baselines achieve similar performance as reported by [Sahoo et al. \(2024\)](#). On LM1B, we obtain a validation perplexity of 27.67 after 1M steps (compared to MDLM’s reported 27.04), while on OWT, we reach 23.07 (versus MDLM’s 23.21).

Minor differences can be expected since estimating the perplexity of diffusion language models involves a Monte-Carlo approximation of the NELBO (1) with finitely many samples. Although we used libraries (e.g PyTorch) with the same version as MDLM, differences in compute environments and underlying software stacks may also contribute to these variations. Since the performance gap is small, we are confident that we used the code of MDLM correctly.

C.1 LM1B

For the LM1B dataset, we employed the `bert-base-uncased` tokenizer with a context length of 128 tokens, padding shorter sequences. Our architecture consisted of a Diffusion Transformer (DiT) with 12 transformer blocks, 12 attention heads, a hidden dimension of 768, and a dropout rate of 0.1. We optimized the model using Adam ([Kingma & Ba, 2017](#)) (learning rate 3e-4, betas of (0.9, 0.999), epsilon 1e-8) without weight decay. We based our implementation on the [official MDLM codebase](#).

Table 3: Latency and throughput for a single forward+backward pass of the MDLMs and PGMs, computed on a single A100-SXM4-80GB GPU. On LM1B, PGM introduces a negligible overhead over MDLM. On OWT, our PGM with 6 encoder and decoder layers and an embedding dimension of 1024 achieves around 75% of the training throughput of MDLM. Recall that at inference, the same PGM is around $5\times$ faster than MDLM.

Model	Forward Pass		Forward + Backward	
	Latency (ms)	Seq/sec	Latency (ms)	Seq/Sec
<i>LM1B (context length 128, batch size 64, trained on 8 GPUs)</i>				
MDLM	0.03 \pm 0.00	1'978.87 \pm 44.21	0.08 \pm 0.00	714.80 \pm 15.47
PGM 6 / 6	0.03 \pm 0.00	1'966.60 \pm 102.14	0.08 \pm 0.00	794.42 \pm 18.81
<i>OpenWebText (context length 1024, batch size 32, trained on 16 GPUs)</i>				
MDLM	0.13 \pm 0.00	233.28 \pm 2.58	0.39 \pm 0.00	80.86 \pm 0.15
PGM 8 / 8	0.17 \pm 0.00	188.07 \pm 0.75	0.47 \pm 0.00	68.04 \pm 0.08
PGM 6 / 6 (dim. 1024)	0.18 \pm 0.00	176.47 \pm 0.65	0.50 \pm 0.00	62.85 \pm 0.19

We trained with a global batch size of 512 across 8 GPUs (2 nodes with 4 GPUs), gradient clipping at 1.0, and a constant learning rate with 2,500 steps of linear warmup. We trained for 1 million steps with an EMA rate of 0.9999. Besides the neural network hyperparameters, the other parameters were unchanged when training the PGM.

C.2 OWT

For the OpenWebText (OWT) dataset, we used the GPT-2 tokenizer with a context length of 1024 tokens. Our architecture consisted of a Diffusion Transformer (DiT) with 12 transformer blocks, 12 attention heads, a hidden dimension of 768, and a dropout rate of 0.1. We optimized the model using Adam (Kingma & Ba, 2017) with a learning rate of 3e-4, betas of (0.9, 0.999), and epsilon of 1e-8, without weight decay. We trained with a global batch size of 512 across 16 GPUs (4 nodes with 4 GPUs). We applied gradient clipping at 1.0 and used a constant learning rate schedule with 2,500 steps of linear warmup. The model was trained for 1 million steps with an EMA rate of 0.9999. Besides the neural network hyperparameters, the other parameters were unchanged when training the PGM.

C.3 IMAGENET

For the ImageNet experiments, we used a pre-trained VQGAN tokenizer (Esser et al., 2021; Besnier et al., 2025), following the setup of Besnier et al. (2025). The images are tokenized into sequences of 1024 tokens. This allowed for a direct comparison between PGM and MaskGIT, both trained in the codebase of Besnier et al. (2025) and the FID is evaluated using the Halton sampler and the confidence sampler. We compute the FID between 50k generated images and the validation set, as Besnier et al. (2025)

All models use 24 transformer blocks. For PGM, we add a GroupSwap layer to enable information exchange between partition groups. We use the same hyperparameters as HaltonMaskGIT for all models, except we reduce the training duration to 500k steps (from 2M) due to computational constraints. All models are trained to be class-conditional, which enables the use of classifier-free guidance to significantly improve performance.

C.4 IMPACT OF NUMERICAL PRECISION ON SAMPLING

Zheng et al. (2025) identified that Masked Diffusion Models often achieve lower Generative Perplexity results because of underflow in the logits when sampling using low precision. The resulting decrease in token diversity can make evaluations based solely on Generative Perplexity misleading. Hence, we always cast the logits to FP64 before sampling.

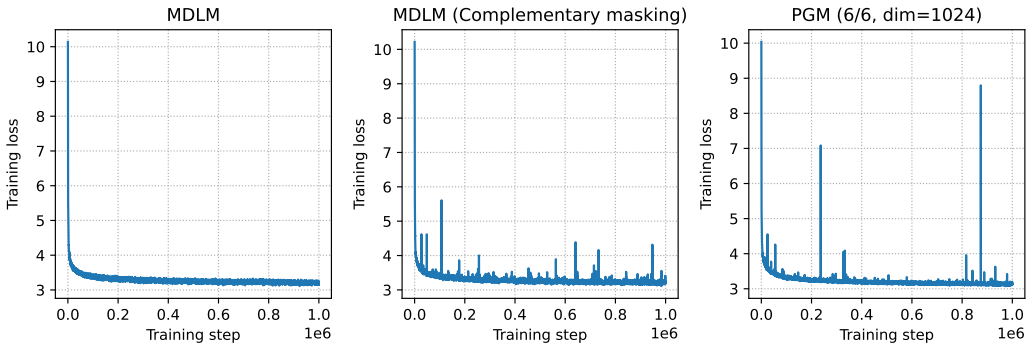


Figure 5: Training loss of MDLM, MDLM with Complementary Masking (Section 5.3) and PGM. Complementary masking seems to introduce spikes in the loss, even though it did not cause the models to diverge.

C.5 SAMPLE-BASED EVALUATION

Generative Perplexity We use the Generative Perplexity to evaluate the quality of samples, following prior work (Lou et al., 2024; Sahoo et al., 2024; Deschenaux & Gulcehre, 2025). The Generative Perplexity measures how well a reference model (in our case, GPT-2 Large) can predict the next token in generated sequences. Specifically, we generate 1'024 samples from each model being evaluated. For each generated sample, we compute the Generative Perplexity using GPT-2 Large as follows:

$$\text{Perplexity} = \exp \left(-\frac{1}{N} \sum_{i=1}^N \log p_{\text{GPT-2 Large}}(x_i | x_{<i}) \right), \quad (10)$$

where L is the length of the sequence, x_i is the i -th token, and $p_{\text{GPT-2 Large}}(x_i | x_{<i})$ is the probability assigned by GPT-2 Large to token x_i given the preceding tokens $x_{<i}$.

Unigram Entropy Unfortunately, a low Generative Perplexity can be achieved by generating repetitive text. To catch such cases, we compute the average unigram entropy of the generated samples:

$$\text{Unigram Entropy} = -\frac{1}{N} \sum_{i=1}^N \sum_{v \in \mathcal{X}} \frac{c(v, \mathbf{x}^{(i)})}{L} \log \frac{c(v, \mathbf{x}^{(i)})}{L}, \quad (11)$$

where \mathcal{X} is the vocabulary, v is a token of the vocabulary, and $c(v, \mathbf{x})$ is the empirical appearance count of the token v in the sequence \mathbf{x} . Low unigram entropy helps us to catch degenerate generation, as shown by Dieleman et al. (2022).

Fréchet Inception Distance and Inception Score On image generation tasks, we evaluate the quality of samples using the Fréchet Inception Distance (FID) (Heusel et al., 2018) and Inception Score (IS) (Salimans et al., 2016). Both metrics are computed using 50'000 images, following the standard practice.

D ADDITIONAL RESULTS

D.1 IMPACT OF CONTEXT LENGTH ON THE EFFECTIVENESS OF COMPLEMENTARY MASKING

There are three key differences between our experiments on LM1B and OWT. First, we used different tokenizers: `bert-base-uncased` for LM1B and GPT2's tokenizer for OWT, following the setup of MDLM (Sahoo et al., 2024). Second, the context lengths differ significantly: 128 tokens for LM1B versus 1024 for OWT. Third, we train on different datasets that might have different characteristics.

We observed that complementary masking helps when training on OWT using a shorter context length of 128 tokens with the GPT-2 tokenizer. Indeed, after 200k training step, the MDLM with

complementary masking achieved a validation PPL of 37.92, outperforming the standard MDLM, which reached 39.90. This suggests that PGMs may not need extra parameters when the sequence length is short. Exploring the use of PGMs in domains where the sequence length is short, such as modeling chemical sequences, is a promising direction for future work.

D.2 MDLM+SDTT vs PGM+SDTT

The precision of logits during sampling can have a significant effect on sample quality, as noted in Section C.4. Hence, we cast all logits to FP64 prior to sampling, unlike the original MDLM and SDTT implementations.

Using higher precision also affects distillation, which compresses two sampling steps into one. As shown in Table 7, models distilled with float32 achieve lower Generative Perplexity than those trained with mixed precision (bf16). We therefore report float32 results in the main body.

D.3 ADDITIONAL RESULTS RESULTS ON IMAGENET

Table 8 and Table 9 show the FID, IS, latency, and throughput for the Confidence and Halton samplers. Overall, the Halton sampler works best for both MaskGIT and PGM. With 32 steps and the confidence-based sampler, PGM 12/12 gets a better FID than MaskGIT and is 3.58 \times faster. With 32 steps and the Halton sampler, PGM has a slightly higher FID than MaskGIT (5.54 vs 5.35), but is 7.5 \times faster. If we increase the number of sampling steps to 64, PGM achieves an FID of 4.56, which is better than MaskGIT, and is 3.92 \times faster. Generally, the 12/12 variant outperforms the 14/10 variant, which suggests that balanced number of layers in the encoder and decoder is beneficial, just as for language modeling (Table 5).

D.4 TRAINING STABILITY

Complementary masking introduces occasional spikes in the training loss in both MDLMs and PGMs, as shown in Figure 5. This phenomenon should be kept in mind when scaling PGMs to larger sizes. Despite these spikes, all runs converged on the first attempt. We observed different precision requirements between models. For loss computations, MDLMs performed best with BF16 precision, while PGMs achieved better results with FP32 precision. Both models use mixed precision within the neural network; the precision difference only affects computations performed outside the model, such as the loss calculation.

D.5 ADDITIONAL DOWNSTREAM TASKS

Table 4 reports additional downstream results as in Deschenaux & Gulcehre (2025), where PGM outperforms MDLM on all but one benchmark, with only a small gap on the latter. We evaluate models with the lm-eval-harness library (Gao et al., 2024), originally designed for autoregressive LMs and adapted here for MDLM. For multiple-choice tasks, lm-eval-harness computes the log-likelihood of each candidate answer \mathbf{y}_i given a prefix \mathbf{x} , i.e., $p(\mathbf{y}_i|\mathbf{x})$, and selects the answer with the highest score.

While lm-eval-harness uses the log-likelihood of the continuation, the NELBO objective (1) bounds the log-likelihood of the *complete* sequence $(\mathbf{x}, \mathbf{y}_i)$. However, we only need to know which continuation achieves the highest log-likelihood, not to compute the exact log-likelihood. Using Bayes' theorem, we note that

$$\log p(\mathbf{y}_i|\mathbf{x}) = \log p(\mathbf{x}, \mathbf{y}_i) - \log p(\mathbf{x}) \propto \log p(\mathbf{x}, \mathbf{y}_i), \quad (12)$$

since $\log p(\mathbf{x})$ is constant with respect to \mathbf{y}_i . Therefore, we can simply evaluate the variational bound on $\log p(\mathbf{x}, \mathbf{y}_i)$ to select the most likely continuation y_i .

D.6 PERFORMANCE ON LONGER CONTEXT LENGTH

Due to the high computational cost, we were unable to train models with context lengths greater than 1024. Nevertheless, we report the latency and throughput of both MDLM and PGM at a context length of 4096. As shown in Table 10, PGM remains substantially faster than MDLM in this setting.

Model	LAMBADA	ARC-e	ARC-c	HSwag	MathQA	PIQA	WinoG
MDLM	38.52	34.26	24.66	31.54	20.70	57.89	51.93
PGM 8 / 8	46.98	37.37	24.06	33.10	21.24	59.09	51.30
PGM 6 / 6 (1024)	41.39	38.80	22.95	33.92	21.71	61.43	54.30

Table 4: Accuracy on downstream tasks. We evaluate MDLM and PGM on LAMBADA, ARC Easy and Challenge, HellaSwag, MathQA, PIQA, and WinoGrande. Both models show comparable performance across tasks. PGM outperforms MDLM on all but one benchmark, where the difference between MDLM and PGM 8 / 8 is small.

E COMPUTATIONAL COSTS

This section presents the computational costs associated with the models reported in this paper. We exclude costs associated with exploratory experiments that yielded inferior results and were not included in this manuscript.

E.1 TRAINING COSTS

Training PGMs is currently slower than training MGMs since we use `torch.sdp` with dense tensor masks. Future work should explore efficient kernels to address this limitation. We measure the latency and throughput using a single NVIDIA A100-SXM4-80GB GPU, with results reported in Table 3. We compute the mean and standard deviation over 100 batches after 2 warmup batches.

The total training duration approximately equals the per-step latency multiplied by the number of steps. Experiments with complementary masking required twice the computational resources due to larger batch sizes and gradient accumulation. Training times for 1M steps varied by dataset: approximately 22 hours for LM1B, 4.5 days for OWT, and 3.8 days for ImageNet.

Despite the current training overhead, we are confident that future work can improve the training efficiency of PGMs, thanks to their block-diagonal attention patterns, once the tokens are grouped together along the sequence-length axis.

E.2 INFERENCE COSTS

We evaluate the inference efficiency of PGMs compared to MDLMs and GPT-2 with KV caching. As shown in Figure 1, PGMs achieve around $5 - 5.5 \times$ improvements in throughput over MDLM while reaching superior Generative Perplexity. For inference measurements, we use a single NVIDIA A100-SXM4-80GB GPU. The efficiency gain stems from the ability of PGMs to process only unmasked tokens during inference, as illustrated in Figure 2. Table 6 compares MDLM and PGMs on the Generative Perplexity, unigram entropy, latency, and throughput. We compute the mean and standard deviation of the latency and throughput over 20 batches after two warmup batches.

E.3 LICENSING

Our code and model artifacts will be released under the MIT license. The OWT dataset (Gokaslan & Cohen, 2019) is available under the Apache License 2.0. We were unable to identify a specific license for the LM1B dataset (Chelba et al., 2014). The images in ImageNet remain the property of their respective copyright holders.

Algorithm 1 Simplified Sampling for PGMs

```

1: Input: Batch size BS, number of steps K, model length L, special BOS index
2: Output: Generated samples x
3: x  $\leftarrow$  empty_tensor(BS, 1) ▷ Initialize
4: x[:, 0]  $\leftarrow$  BOS ▷ Set BOS as first token
5: k  $\leftarrow$  L/K ▷ Number of tokens to denoise at each step
6: decoded_positions  $\leftarrow$  zeros(BS, 1) ▷ Keep track of already-decoded and positions to decode
7: positions_to_decode  $\leftarrow$  1 + rand_row_perm(BS, L-1) ▷ Each row is a permutation of {1, ..., L}
8: for _ in range(K) do
9:   pos_to_decode  $\leftarrow$  positions_to_decode[:, :k] ▷ Random positions to be predicted
10:  new_values  $\leftarrow$  pgm_predict(x, decoded_positions, pos_to_decode)
11:  x  $\leftarrow$  concat([x, new_values], dim=1) ▷ Add new values to the sequence length dimension
12:  decoded_positions  $\leftarrow$  concat([decoded_positions, pos_to_decode], dim=1)
13:  positions_to_decode  $\leftarrow$  positions_to_decode[:, k:] ▷ Remove the k decoded positions
14: end for
15: out  $\leftarrow$  reorder(x, decoded_positions) ▷ Sort based on positions
16: return out

```

Algorithm 2 MDLM-equivalent sampling for PGMs.

```

1: Input: Batch size BS, number of steps K, model length L, special BOS index
2: Output: Generated samples x
3: x  $\leftarrow$  empty_tensor(BS, 1) ▷ Initialize
4: x[:, 0]  $\leftarrow$  BOS ▷ Set BOS as first token
5: k  $\leftarrow$  L/K ▷ Number of tokens to denoise at each step
6: clean_positions  $\leftarrow$  zeros(BS, 1) ▷ Keep track of clean and noisy positions
7: concrete_lengths  $\leftarrow$  ones(BS, 1) ▷ Keep track of the actual length of each sequence (some are padded).
8: noisy_positions  $\leftarrow$  1 + rand_row_perm(BS, L-1)
9: for _ in range(K) do
10:   n_denoise_per_seq, noisy_pos_input  $\leftarrow$  sample_noisy(noisy_positions, k) ▷ Algorithm Algo. 3
11:   new_values  $\leftarrow$  pgm_predict(x, clean_positions, noisy_pos_input)
12:   x, clean_positions, noisy_positions, concrete_lengths  $\leftarrow$  extract_predictions(▷ Algorithm Algo. 4
13:     x,
14:     clean_positions,
15:     noisy_positions,
16:     noisy_pos_input,
17:     concrete_lengths,
18:     n_denoise_per_seq,
19:     new_values)
20: end for
21: out  $\leftarrow$  reorder(x, clean_positions) ▷ Sort based on clean_positions
22: return out

```

Algorithm 3 Sample the number of tokens to denoise from a binomial distribution and pad the input.

```

1: Input: Noisy positions tensor, probability of denoising prob_denoise, model length L, concrete lengths tensor
2: Output: Noisy positions to denoise
3: n_denoise_per_seq  $\leftarrow$  binomial(BS, L, prob_denoise) ▷ Sample from binomial distribution
4: n_denoise_per_seq  $\leftarrow$  min(n_denoise_per_seq, L - concrete_lengths) ▷ Don't denoise more than available
5: denoise_seq_len  $\leftarrow$  max(n_denoise_per_seq, 0) ▷ Maximum number of tokens to denoise
6: if denoise_seq_len = 0 then
7:   return empty_tensor() ▷ Nothing to denoise
8: end if
9: noisy_pos_input  $\leftarrow$  noisy_positions[:, :denoise_seq_len] ▷ Some predictions won't be used
10: return n_denoise_per_seq, noisy_pos_input

```

Algorithm 4 Extract the correct number of predictions per sequence

```

1: Input: x, concrete_lengths, n_denoise_per_seq, denoised_token_values, clean_positions,
   noisy_positions, noisy_pos_input
2: Output: Updated x, clean_positions, noisy_positions, concrete_lengths
3: new_concrete_lengths  $\leftarrow$  concrete_lengths + n_denoise_per_seq     $\triangleright$  Update sequence lengths
4: n_tok_to_add  $\leftarrow$  max(new_concrete_lengths) - shape(x, 1)       $\triangleright$  Calculate padding needed
5: if n_tok_to_add  $> 0$  then
6:   pad  $\leftarrow$  zeros(BS, n_tok_to_add)                                 $\triangleright$  Create padding tensor
7:   x  $\leftarrow$  concat(x, pad, dim=1)                                     $\triangleright$  Pad the sequences
8:   clean_positions  $\leftarrow$  concat(clean_positions, pad, dim=1)       $\triangleright$  Pad the positions
9: end if
10: for i in range(BS) do
11:   if n_denoise_per_seq[i] = 0 then
12:     continue
13:   end if
14:   x[i, concrete_lengths[i]:new_concrete_lengths[i]]  $\leftarrow$ 
15:     denoised_token_values[i, :n_denoise_per_seq[i]]
16:   clean_positions[i, concrete_lengths[i]:new_concrete_lengths[i]]  $\leftarrow$ 
17:     noisy_pos_input[i, :n_denoise_per_seq[i]]
18:   noisy_positions[i, :shape(noisy_positions, 1) - n_denoise_per_seq[i]]  $\leftarrow$ 
19:     noisy_positions[i, n_denoise_per_seq[i]:]
20: end for
21: return x, clean_positions, noisy_positions, new_concrete_lengths

```

Model (LM1B)	Val. PPL \downarrow	Model (OWT)	Val. PPL \downarrow
<i>200k steps</i>		<i>200k steps</i>	
MDLM	34.29	MDLM	25.35
MDLM (Compl. masking)	30.87	MDLM (Compl. masking)	25.32
PGM 8 / 4	32.83	PGM 6 / 6	26.96
PGM 10 / 2	33.55	PGM 8 / 8	25.10
PGM 4 / 8	32.84	PGM 10 / 6	25.19
PGM 6 / 6	32.69	PGM 6 / 6 (dim. 1024)	23.75
PGM 6 / 6 (lsm)	32.70		
PGM 6 / 6 (mean)	33.89		
<i>1M steps</i>		<i>IM steps</i>	
MDLM	27.67	MDLM	23.07
MDLM (Compl. masking)	25.72	MDLM (Compl. masking)	22.98
PGM 6 / 6	26.80	PGM 8 / 8	22.61
		PGM 6 / 6 (dim. 1024)	21.43

Table 5: Perplexity evaluations. Validation perplexity of the Masked Diffusion Language Model (MDLM) and PGMs (ours) on LM1B and OpenWebText (OWT). The row *MDLM (Compl. masking)* denotes an MDLM trained with the complementary masking strategy discussed in Section 5.3. The row *PGM k / m* denotes a PGM with *k* encoder and *m* decoder layers, and we highlighted the best PGM results in gray. *lsm* and *mean* denote the *logsumexp* and *mean* queries initializations (Section 4). **Takeaway:** using the same number of layers in the encoder and decoder, and data-independent queries performed best. On LM1B, our PGM reaches 1.95 lower perplexity than MDLM after 1M steps. On OWT, we grow the embedding dimension or the number of layers to outperform OWT.

Table 6: Sample quality and efficiency on OpenWebText with different numbers of sampling steps. We generate sequences of 1024 tokens with a batch size of 32 to measure the latency and throughput. PGM 6 / 6 with a hidden dimension of 1024 and uniform sampling achieves at least a 5× latency and throughput improvement over MDLM, with better Generative Perplexity and matching entropy.

Model	Gen. PPL ↓	Entropy ↑	Latency ↓ (ms)	Throughput ↑ (tok/s)
<i>MDLM</i>				
32 steps	192.31	5.73	8.037 ± 0.01	$4'077.08 \pm 3.06$
64 steps	142.58	5.69	15.82 ± 0.01	$2'070.67 \pm 0.69$
128 steps	122.89	5.67	31.41 ± 0.01	$1'043.22 \pm 0.16$
256 steps	113.96	5.66	62.54 ± 0.01	523.90 ± 0.06
512 steps	109.05	5.64	124.94 ± 0.16	262.26 ± 0.33
1024 steps	106.75	5.64	249.31 ± 0.11	131.42 ± 0.05
<i>PGM 8 / 8 (uniform sampling)</i>				
32 steps	189.02	5.73	1.55 ± 0.01	$21'120.99 \pm 83.59$
64 steps	143.79	5.69	3.00 ± 0.01	$10'914.91 \pm 41.69$
128 steps	122.21	5.66	5.86 ± 0.02	$5'585.57 \pm 24.49$
256 steps	112.48	5.65	11.64 ± 0.03	$2'814.99 \pm 9.33$
512 steps	108.76	5.64	22.98 ± 0.02	$1'425.89 \pm 1.61$
1024 steps	107.03	5.63	45.84 ± 0.03	714.71 ± 0.50
<i>PGM 8 / 8 (non uniform sampling)</i>				
32 steps	194.09	5.73	2.07 ± 0.02	$15'764.09 \pm 192.12$
64 steps	143.60	5.69	3.90 ± 0.07	$8'405.14 \pm 158.01$
128 steps	124.38	5.67	7.41 ± 0.08	$4'419.77 \pm 53.27$
256 steps	116.85	5.66	14.73 ± 0.19	$2'223.6372 \pm 28.47$
512 steps	111.11	5.64	28.15 ± 0.32	$1'163.79 \pm 13.25$
1024 steps	108.24	5.63	54.62 ± 0.66	599.97 ± 7.27
<i>PGM 6 / 6 (dim. 1024, uniform sampling)</i>				
32 steps	185.16	5.73	1.59 ± 0.01	$20'569.99 \pm 95.63$
64 steps	138.87	5.70	3.03 ± 0.01	$10'805.31 \pm 14.11$
128 steps	116.95	5.67	5.93 ± 0.01	$5'518.09 \pm 13.46$
256 steps	108.51	5.65	11.77 ± 0.01	$2'782.78 \pm 3.46$
512 steps	101.94	5.63	23.25 ± 0.01	$1'408.88 \pm 1.05$
1024 steps	99.64	5.62	46.31 ± 0.02	707.52 ± 0.34
<i>PGM 6 / 6 (dim. 1024, non-uniform sampling)</i>				
32 steps	191.30	5.74	2.12 ± 0.07	$15'415.56 \pm 467.20$
64 steps	138.67	5.69	3.940 ± 0.06	$8'318.72 \pm 135.47$
128 steps	118.17	5.67	7.60 ± 0.09	$4'311.80 \pm 54.92$
256 steps	108.93	5.65	14.84 ± 0.20	$2'207.71 \pm 29.71$
512 steps	105.41	5.64	28.56 ± 0.33	$1'147.17 \pm 13.47$
1024 steps	102.93	5.62	55.50 ± 0.36	590.37 ± 3.85

Table 7: Generative perplexity of MDLM and PGM after distillation with varying precision.

Model	Gen. PPL \downarrow	Entropy \uparrow	Latency \downarrow (ms)	Throughput \uparrow (tok/s)
<i>MDLM + SDTT (loss in BF16)</i>				
32 steps	66.26	5.49	8.037 ± 0.01	$4'077.08 \pm 3.06$
64 steps	53.98	5.46	15.82 ± 0.01	$2'070.67 \pm 0.69$
128 steps	48.02	5.44	31.41 ± 0.01	$1'043.22 \pm 0.16$
256 steps	45.86	5.42	62.54 ± 0.01	523.90 ± 0.06
512 steps	44.21	5.40	124.94 ± 0.16	262.26 ± 0.33
1024 steps	43.19	5.38	249.31 ± 0.11	131.42 ± 0.05
<i>MDLM + SDTT (loss in FP32)</i>				
32 steps	61.65	5.46	8.037 ± 0.01	$4'077.08 \pm 3.06$
64 steps	50.65	5.43	15.82 ± 0.01	$2'070.67 \pm 0.69$
128 steps	45.06	5.40	31.41 ± 0.01	$1'043.22 \pm 0.16$
256 steps	41.70	5.37	62.54 ± 0.01	523.90 ± 0.06
512 steps	40.63	5.36	124.94 ± 0.16	262.26 ± 0.33
1024 steps	39.50	5.32	249.31 ± 0.11	131.42 ± 0.05
<i>PGM 6/6 (dim. 1024) + SDTT (loss in BF16)</i>				
32 steps	91.61	5.56	1.59 ± 0.01	$20'569.99 \pm 95.63$
64 steps	72.73	5.52	3.03 ± 0.01	$10'805.31 \pm 14.11$
128 steps	63.83	5.49	5.93 ± 0.01	$5'518.09 \pm 13.46$
256 steps	58.74	5.47	11.77 ± 0.01	$2'782.78 \pm 3.46$
512 steps	58.77	5.47	23.25 ± 0.01	$1'408.88 \pm 1.05$
1024 steps	56.47	5.46	46.31 ± 0.02	707.52 ± 0.34
<i>PGM 6/6 (dim. 1024) nucleus (p=0.9) + SDTT (loss in BF16)</i>				
32 steps	68.33	5.50	1.74 ± 0.01	$18'866.12 \pm 18.35$
64 steps	53.88	5.45	3.18 ± 0.01	$10'307.16 \pm 6.58$
128 steps	46.99	5.42	6.10 ± 0.01	$5'375.20 \pm 2.40$
256 steps	43.22	5.40	11.95 ± 0.01	$2'742.74 \pm 1.32$
512 steps	42.79	5.39	23.63 ± 0.01	$1'386.79 \pm 0.69$
1024 steps	40.99	5.38	46.83 ± 0.02	699.80 ± 0.24
<i>PGM 6/6 (dim. 1024) + SDTT (loss in FP32)</i>				
32 steps	84.97	5.52	1.74 ± 0.01	$20'569.99 \pm 95.63$
64 steps	67.60	5.49	3.18 ± 0.01	$10'805.31 \pm 14.11$
128 steps	60.06	5.47	6.10 ± 0.01	$5'518.09 \pm 13.46$
256 steps	55.97	5.45	11.95 ± 0.01	$2'782.78 \pm 3.46$
512 steps	54.13	5.44	$1'408.88 \pm 1.05$	$1'408.88 \pm 1.05$
1024 steps	52.77	5.44	46.83 ± 0.02	707.52 ± 0.34
<i>PGM 6/6 (dim. 1024) nucleus (p=0.9) + SDTT (loss in FP32)</i>				
32 steps	63.46	5.45	1.59 ± 0.01	$18'866.12 \pm 18.35$
64 steps	49.94	5.41	3.03 ± 0.01	$10'307.16 \pm 6.58$
128 steps	43.84	5.39	5.93 ± 0.01	$5'375.20 \pm 2.40$
256 steps	40.76	5.36	11.77 ± 0.01	$2'742.74 \pm 1.32$
512 steps	39.46	5.36	23.25 ± 0.01	$1'386.79 \pm 0.69$
1024 steps	38.81	5.35	46.31 ± 0.02	699.80 ± 0.24
<i>PGM 8/8 + SDTT (loss in BF16)</i>				
32 steps	102.64	5.54	1.55 ± 0.01	$21'120.99 \pm 83.59$
64 steps	82.93	5.50	3.00 ± 0.01	$10'914.91 \pm 41.69$
128 steps	73.19	5.48	5.86 ± 0.02	$5'585.57 \pm 24.49$
256 steps	70.30	5.47	11.64 ± 0.03	$2'814.99 \pm 9.33$
512 steps	68.07	5.46	22.98 ± 0.02	$1'425.89 \pm 1.61$
1024 steps	65.87	5.44	45.84 ± 0.03	714.71 ± 0.50
<i>PGM 8/8 + SDTT (loss in FP32)</i>				
32 steps	87.64	5.51	1.55 ± 0.01	$21'120.99 \pm 83.59$
64 steps	70.47	5.48	3.00 ± 0.01	$10'914.91 \pm 41.69$
128 steps	62.66	5.46	5.86 ± 0.02	$5'585.57 \pm 24.49$
256 steps	59.38	5.45	11.64 ± 0.03	$2'814.99 \pm 9.33$
512 steps	57.57	5.44	22.98 ± 0.02	$1'425.89 \pm 1.61$
1024 steps	56.12	5.44	45.84 ± 0.03	714.71 ± 0.50

Table 8: Sample quality and efficiency on ImageNet for different numbers of sampling steps using the *Confidence-based* sampler. We generate images in batches of 32 to measure throughput, and use a batch size of 1 to measure latency. Throughput is lower with CFG because each step requires two forward passes (conditional and unconditional). The throughput and latency are averaged over 10 batches.

Model	FID ↓	IS ↑	Latency ↓ (ms)	Throughput ↑ (img/s)
<i>MaskGIT (32 steps; 458M)</i>				
w = 0	14.30	82.41	0.70	2.05
w = 1	7.80	151.62	1.21	1.05
w = 2	6.78	208.92	1.21	1.05
w = 3	<u>7.37</u>	255.69	1.21	1.05
w = 4	7.46	289.93	1.21	1.05
w = 5	9.61	250.86	1.21	1.05
w = 6	21.68	149.61	1.21	1.05
<i>MaskGIT (64 steps; 458M)</i>				
w = 0	15.62	79.23	1.39	1.03
w = 1	9.40	140.48	2.41	0.52
w = 2	<u>8.06</u>	195.35	2.41	0.52
w = 3	<u>8.19</u>	239.89	2.41	0.52
w = 4	7.61	267.26	2.41	0.52
w = 5	11.44	202.92	2.41	0.52
w = 6	26.41	113.63	2.41	0.52
<i>PGM 12 / 12 (32 steps; 464M)</i>				
w = 0	18.77	67.22	1.04	6.86
w = 1	8.96	135.03	1.08	3.76
w = 2	6.67	201.66	1.08	3.76
w = 3	<u>7.09</u>	255.43	1.08	3.76
w = 4	8.30	290.18	1.08	3.76
w = 5	9.59	307.52	1.08	3.76
w = 6	10.84	313.27	1.08	3.76
<i>PGM 12 / 12 (64 steps; 464M)</i>				
w = 0	19.45	64.44	2.04	3.52
w = 1	10.08	124.90	2.04	1.90
w = 2	7.35	188.77	2.04	1.90
w = 3	<u>7.39</u>	238.31	2.04	1.90
w = 4	8.13	276.55	2.04	1.90
w = 5	9.18	297.44	2.04	1.90
w = 6	10.38	302.29	2.04	1.90
<i>PGM 14 / 10 (32 steps; 464M)</i>				
w = 0	21.97	60.07	1.04	7.09
w = 1	11.24	121.39	1.04	3.90
w = 2	<u>8.05</u>	183.20	1.04	3.90
w = 3	7.76	232.62	1.04	3.90
w = 4	8.47	263.73	1.04	3.90
w = 5	9.39	288.60	1.04	3.90
w = 6	10.40	291.46	1.04	3.90
<i>PGM 14 / 10 (64 steps; 464M)</i>				
w = 0	22.74	56.77	2.03	3.63
w = 1	12.32	112.98	2.04	1.97
w = 2	8.80	171.11	2.04	1.97
w = 3	8.11	219.33	2.04	1.97
w = 4	<u>8.44</u>	253.10	2.04	1.97
w = 5	9.12	270.16	2.04	1.97
w = 6	9.90	279.00	2.04	1.97

Table 9: Sample quality and efficiency on ImageNet for different numbers of sampling steps using the *Halton* sampler. We generate images in batches of 32 to measure throughput, and use a batch size of 1 to measure latency. Throughput is lower with CFG because each step requires two forward passes (conditional and unconditional). The throughput and latency are averaged over 10 batches.

Model	FID ↓	IS ↑	Latency ↓ (ms)	Throughput ↑ (img/s)
<i>MaskGIT (32 steps; 458M)</i>				
w = 0	25.72	57.70	0.70	2.02
w = 1	5.35	267.49	1.21	1.05
w = 2	<u>12.82</u>	365.36	1.21	1.05
w = 3	17.24	408.30	1.21	1.05
w = 4	15.65	<u>365.97c</u>	1.21	1.05
w = 5	25.33	182.14	1.21	1.05
w = 6	48.97	74.74	1.21	1.05
<i>MaskGIT (64 steps; 458M)</i>				
w = 0	18.61	69.68	1.39	1.03
w = 1	6.76	283.96	2.41	0.52
w = 2	<u>14.97</u>	<u>372.74</u>	2.41	0.52
w = 3	18.30	410.60	2.41	0.52
w = 4	16.18	312.75	2.41	0.52
w = 5	32.69	126.69	2.41	0.52
w = 6	60.12	51.40	2.41	0.52
<i>PGM 12 / 12 (32 steps; 464M)</i>				
w = 0	22.59	66.32	1.03	13.44
w = 1	10.21	134.22	1.03	7.93
w = 2	<u>6.04</u>	203.28	1.03	7.93
w = 3	5.54	263.53	1.03	7.93
w = 4	6.38	311.53	1.03	7.93
w = 5	7.58	<u>345.18</u>	1.03	7.93
w = 6	8.83	372.07	1.03	7.93
<i>PGM 12 / 12 (64 steps; 464M)</i>				
w = 0	16.19	79.26	1.96	7.17
w = 1	6.67	151.44	2.01	4.12
w = 2	4.56	218.98	2.01	4.12
w = 3	<u>4.98</u>	276.16	2.01	4.12
w = 4	6.47	322.53	2.01	4.12
w = 5	7.95	<u>352.56</u>	2.01	4.12
w = 6	9.47	379.39	2.01	4.12
<i>PGM 14 / 10 (32 steps; 464M)</i>				
w = 0	25.42	62.11	1.01	12.70
w = 1	11.57	128.22	1.00	7.37
w = 2	6.60	196.56	1.00	7.37
w = 3	5.55	253.76	1.00	7.37
w = 4	<u>6.00</u>	301.66	1.00	7.37
w = 5	7.04	<u>334.29</u>	1.00	7.37
w = 6	8.16	365.56	1.00	7.37
<i>PGM 14 / 10 (64 steps; 464M)</i>				
w = 0	18.03	75.40	1.93	6.69
w = 1	7.77	144.26	1.99	3.80
w = 2	4.76	212.39	1.99	3.80
w = 3	<u>4.85</u>	268.55	1.99	3.80
w = 4	5.88	309.88	1.99	3.80
w = 5	7.23	<u>342.40</u>	1.99	3.80
w = 6	8.63	366.57	1.99	3.80

Table 10: Throughput (TP) of MDLM and PGM with a context length of 4096, for varying number of inference steps. PGM is significantly faster than MDLM.

Model	TP (4096)	TP (1024)	TP (256)	TP (64)
MDLM	30.45 ± 0.06	121.25 ± 0.02	483.53 ± 0.25	$1'912.16 \pm 1.44$
PGM 8/8	128.99 ± 0.23	697.36 ± 32.83	$2'216.91 \pm 3.06$	$8'203.82 \pm 6.60$
PGM 6/6 (dim=1024)	129.01 ± 0.67	706.65 ± 36.23	$2'146.60 \pm 15.12$	$8'175.69 \pm 7.85$